Materials Research Proceedings 59 (2026) 17-24 https://doi.org/10.21741/9781644903957-3

Eco-Friendly Activation of Palm Kernel Shell Carbon using Calcium Chloride from Cockle Shells

Mohamad Razlan MD RADZI[1,a], Nor Adilla RASHIDI[1,b *]

[1]HICoE—Centre for Biofuel and Biochemical Research, Institute of Sustainable Energy and Resources (ISER), Department of Chemical Engineering, Universiti Teknologi PETRONAS, Seri Iskandar, Perak 32610, Malaysia

[a]razlan.radzi@utp.edu.my, [b]adilla.rashidi@utp.edu.my

Keywords: Biomass Utilization, Heavy Metal Adsorption

Abstract. The study aimed to develop a sustainable, low-cost method for removing heavy metals such as iron (Fe) from wastewater by producing activated carbon from palm kernel shells, activated with calcium chloride derived from waste cockle shells. Using a Taguchi L_9 orthogonal array, nine samples were synthesized by varying temperature (500-700°C), heating time (60-120 min), and calcium chloride concentration (0.25-1M). The carbon yield was affected mainly by temperature and time, with excessive values causing ash formation. The best-performing sample was tested for Pb adsorption using atomic absorption spectrometry (AAS). Results showed that higher adsorbent dosage increased removal efficiency, while higher metal concentrations reduced it. Longer contact times initially improved adsorption but eventually reached equilibrium.

Introduction

Cockle is a popular seafood in Malaysia and a key aquaculture product. However, the discarded shells, which constitute nearly two-thirds of the biomass, pose environmental concerns due to slow biodegradation and pollution risks. To mitigate this, studies have explored reusing cockle shells as low-cost adsorbents and other products [1]. Rich in calcium carbonate ($CaCO_3$) up to 95%, cockle shells offer a sustainable alternative to mined limestone, reducing the ecological damage linked to conventional extraction [2].

Activated carbon is a highly porous material derived from carbon-rich sources such as bamboo, coconut husks, and palm kernel shells (PKS). It is widely used in environmental and industrial applications due to its exceptional adsorption capacity, high surface area, and chemical stability [3]. Common applications include water and air purification, wastewater treatment, and serving as catalyst supports. Activated carbon's effectiveness stems from its extensive pore structure and the presence of surface functional groups such as carboxyl, carbonyl, phenol, lactone, and quinone, which play key roles in binding and adsorbing various contaminants [4]. It is particularly valued for its ability to withstand harsh chemical environments and its high affinity for a wide range of pollutants [5].

The production of activated carbon from biomass can be enhanced through chemical activation techniques. In this method, calcium chloride derived from cockle shells is used to impregnate the palm kernel shell biomass, promoting pore development and enhancing the adsorptive properties of the final product [6]. Utilizing calcium chloride from waste cockle shells not only adds value to a previously discarded by-product but also reduces dependence on conventional, often hazardous and costly activating agents such as phosphoric acid or zinc chloride. This approach offers a more economical, environmentally friendly, and sustainable pathway for producing high-performance activated carbon. Furthermore, the synthesized activated carbon was later evaluated for its ability to remove iron (Fe) from aqueous solutions, highlighting its potential in treating Fe-contaminated wastewater.

Content from this work may be used under the terms of the Creative Commons Attribution 3.0 license. Any further distribution of this work must maintain attribution to the author(s) and the title of the work, journal citation and DOI. Published under license by Materials Research Forum LLC.

Materials and Methods

Cockle shells were collected from local stores in Seri Iskandar, Perak, cleaned, dried at 110°C, ground, and sieved to 100 µm. Palm kernel shells from FELCRA Nasaruddin Belia in Bota, Perak, were similarly cleaned, dried, ground, and sieved. Calcium chloride ($CaCl_2$) was synthesized by reacting cockle shell powder with hydrochloric acid (0.5–2 M), producing $CaCl_2$ solutions of 0.25-1 M after filtration.

Five grams of palm kernel shell were impregnated overnight with 100 mL of the $CaCl_2$ solution, dried, and calcined under conditions defined by a Taguchi L_9 orthogonal array. The resulting activated carbon was washed with 10% HCl and deionized water until neutral pH, then its yield was calculated using formula in Eq. 1.

$$\text{Yield (\%)} = \frac{\text{weight of AC after washing (g)}}{\text{inital PKS weight (g)}} \times 100\% \quad (1)$$

The activated carbon's adsorption performance for iron (Fe) removal was tested using Fe(III) nitrate solutions. Experiments varied three parameters: adsorbent dosage (0.005-0.1 g), initial Fe concentration (20-120 ppm), and contact time (30-180 min) at 30°C. After adsorption, samples were filtered and analysed via Atomic Absorption Spectrometry (AAS, Agilent 240FS). The adsorption capacity (q_e) was determined using Eq. 2 based on Fe concentrations before and after treatment, where q_e is the adsorption capacity in mg/g, C_o is the initial Fe concentration in mg/L, C_e is the equilibrium Fe concentration in mg/L, V is the volume of solution in L and m is the mass of adsorbent in g.

$$q_e = \frac{(C_0 - C_e) \times V}{m} \quad (2)$$

Results and Discussion

The section was subdivided into multiple subsections discussing about optimization of activated carbon synthesis using Taguchi L_9 orthogonal array based on pyrolysis temperature, pyrolysis time and concentration of calcium chloride, followed by characterization of activated carbon and lastly effect of initial Fe concentration, adsorbent dosage and contact time on Fe adsorption. Three key parameters, calcium chloride molarity (0.25-1 M), calcination temperature (500-700°C), and calcination time (60-120 min), were optimized using the Taguchi L_9 orthogonal array to maximize activated carbon yield from palm kernel shells (PKS). The yield was determined by comparing the final product weight to the initial biomass weight.

Table 1 *Yield calculation of activated carbon.*

	Parameters			Weight (g)			
Run	M	Temp. (°C)	Time (min)	PKS	Pyro	Wash	Yield (%)
1	0.25	500	60	5.012	0.31	0.276	5.51
2	0.25	600	90	5.009	0.07	0.031	0.62
3	0.25	700	120	5.005	0.06	0.024	0.48
4	0.5	500	90	5.006	0.55	0.392	7.83
5	0.5	600	120	5.016	0.07	0.059	1.18
6	0.5	700	60	5.013	0.15	0.097	1.93
7	1	500	120	5.009	0.20	0.19	3.79
8	1	600	60	5.011	0.06	0.036	0.72
9	1	700	90	5.006	0.04	0.032	0.64

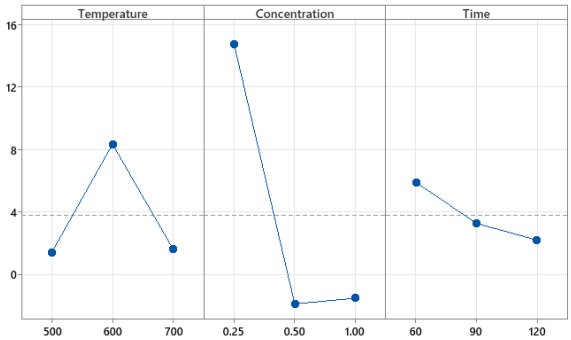


Figure 1 *Signal to noise ratio (SNR) plot.*

Table 1 shows that yield decreases with increasing temperature and time, due to greater decomposition of volatile components. The highest yield of 7.83% occurred at moderate conditions (M = 0.5, 500°C and 90 min), while the lowest yield of 0.48% was at harsher conditions but lower concentrations (M = 0.25, 700 °C and 120 min). This indicates that milder activation favours higher carbon recovery, whereas harsher conditions cause more material loss. From the yield, Taguchi analysis using Minitab and signal-to-noise (S/N) ratios identified the optimal conditions as 600 °C, 0.25 M calcium chloride, and 60 min as observed in Fig. 1. These settings provided the best balance between thermal decomposition and chemical activation, resulting in efficient pore formation, minimal carbon loss, and the highest overall yield. [7].

Characteristics of activated carbon

The FTIR spectrum of the synthesized activated carbon of 600°C, 0.25M calcium chloride, 60 min in Fig. 2 confirms the presence of several characteristic functional groups typically associated with carbonaceous materials. Comparison has shown that the spectrum is almost a duplicate of FTIR spectrum of activated carbon in [8]. A broad absorption band around 3397 cm^{-1} is attributed to O–H stretching vibrations, indicating the presence of hydroxyl groups, which may originate from residual moisture or phenolic compounds commonly retained on the surface of activated carbon due to its high porosity and surface area [9].

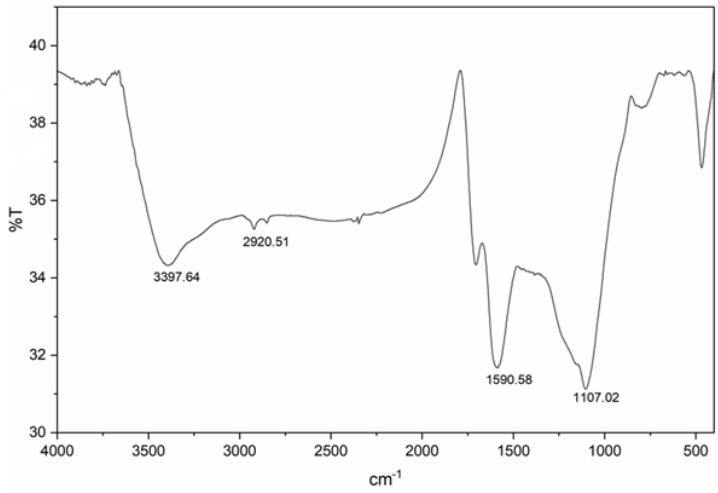


Figure 2 *FTIR spectra of synthesized activated carbon.*

The absorption peak near 2920 cm^{-1} corresponds to C–H stretching vibrations of aliphatic hydrocarbons, suggesting that remnants of lignin or cellulose from the original palm kernel shell precursor may still be present despite pyrolysis [8]. A distinct band near 1590 cm^{-1} is assigned to C=C stretching vibrations within aromatic ring structures, indicating the formation of aromatic

domains during thermal treatment. Additionally, a peak around 1105 cm^{-1} is associated with C–O stretching vibrations, reflective of the presence of ether, alcohol, or phenolic groups on the carbon surface. Finally, absorption bands in the 670-870 cm^{-1} region are characteristic of aromatic C–H out-of-plane bending, further confirming the development of aromatic ring structures during the carbonization process.

SEM analysis in Fig. 3a revealed that the synthesized activated carbon exhibited compact, spherical, and sub-spherical particles with well-defined boundaries and a high degree of structural uniformity. At higher magnification in Fig. 3b, a dense distribution of circular micropores was clearly visible, although the pore sizes appeared slightly smaller compared to those reported in [10]. This observation confirms the successful development of a well-formed porous network, which is essential for enhancing surface area and improving adsorption efficiency. The particles were closely packed with limited large voids, while the presence of small inter-particle gaps suggested additional mesoporosity that could facilitate better diffusion of adsorbates within the material. Minor surface irregularities and debris were observed, possibly originating from residual ash, unreacted precursor material, or mechanical handling during processing.

The EDX analysis in Table 2 further supported the successful synthesis of carbon-rich material, showing that carbon (C) was the predominant element at 73.13%, followed by oxygen (O) at 25.23%, with smaller amounts of silicon (Si) at 1.52% and sulphur (S) at 0.12%.

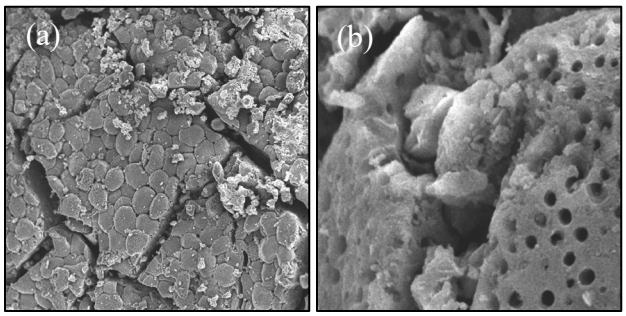


Figure 3 *FESEM micrograph of activated carbon at (a) 500x and (b) 50Kx.*

The high carbon content reflects an effective carbonization process and the efficient removal of non-carbon elements during activation. The presence of oxygen is attributed to surface functional groups such as hydroxyl, carbonyl, and carboxyl, which are known to enhance surface reactivity and adsorption performance. Trace amounts of Si and S may have originated from the raw biomass or minor impurities introduced during activation.

Table 2 *Elemental composition, BET area, pore volume and pore size of activated carbon.*

Elements	Weight %	Parameters	Value
Carbon	73.13	Surface Area (m^2/g)	435.64
Oxygen	25.23	Pore volume (cm^3/g)	0.27
Silicon	1.52	Pore size (nm)	2.48
Sulphur	0.12		

Overall, the elemental composition confirms that the synthesized activated carbon met the SNI 06-3730-1995 standard, with a carbon content exceeding the minimum requirement of 65%, thereby validating its suitability for adsorption and other environmental applications [11].

BET analysis in Table 2 revealed that the synthesized activated carbon exhibited a high specific surface area of 435.64 m^2/g, a total pore volume of 0.27 cm^3/g, and an average pore diameter of 2.48 nm, indicating a predominantly mesoporous structure suitable for adsorption applications

[12]. Such characteristics are advantageous for accommodating larger adsorbate molecules and support potential applications in wastewater treatment, gas separation, and catalysis.

Adsorption of Fe

After optimizing the activated carbon synthesis parameters and conducting its characterization, adsorption experiments were performed to examine the effects of adsorbent dosage, initial Fe concentration, and contact time. The results, summarized in Table 3, revealed distinct trends in Fe removal efficiency for each parameter.

Table 3 *Effects of activated carbon dosage, initial Fe concentration and contact time on* q_e.

Parameters	C_o (mg/L)	C_e (mg/L)	% Removal	q_e (mg/g)
0.005 g	100	77.48	22.52	450.4
0.01 g	100	68.33	31.67	317
0.02 g	100	62.18	37.82	189.1
0.1 g	100	56.09	43.91	43.9
20 ppm	20	4.87	75.65	151.3
40 ppm	40	23.65	40.88	163.5
60 ppm	60	37.49	37.52	225.1
80 ppm	80	50.09	37.39	299.1
100 ppm	100	68.45	31.55	315.5
120 ppm	120	90.13	24.89	299
30 min	100	69.01	30.99	309.9
60 min	100	68.27	31.73	317.3
90 min	100	67.08	32.92	329.2
120 min	100	66.65	33.35	333.5
150 min	100	66.57	33.43	334.3
180 min	100	66.48	33.52	335.2

In Fig. 4, increasing adsorbent dosage enhanced overall Fe removal, with equilibrium concentration (C_e) decreasing from 77.48 mg/L at 0.005 g to 56.09 mg/L at 0.1 g. However, adsorption capacity (q_e) declined from 450.4 mg/g to 43.9 mg/g, reflecting reduced efficiency at higher dosages due to particle aggregation and site overlap [13].

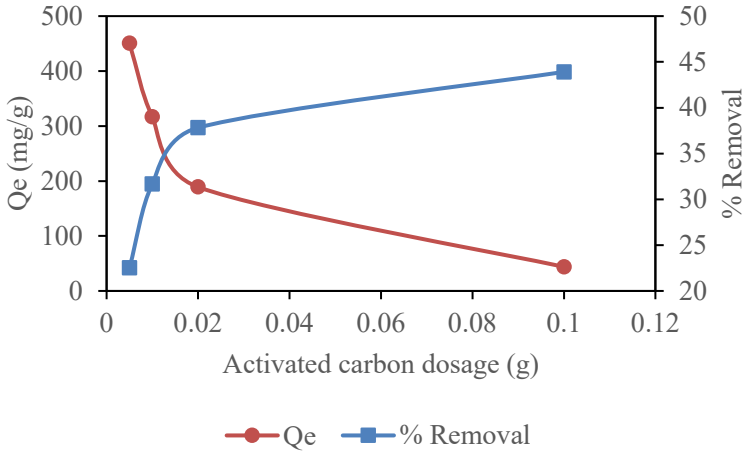


Figure 4 *Effect of activated carbon dosage on adsorption capacity and % removal of Fe.*

The percentage of Fe removal increased from 22.52% to 43.91% as dosage rose, indicating that additional surface area and active sites improved overall metal removal [14]. These results

highlight the need for dosage optimization to achieve an effective balance between Fe removal efficiency and adsorbent utilization.

Fig. 5 shows the effect of initial Fe concentration on the adsorption performance of the activated carbon. The results show that increasing the initial Fe concentration improves q_e, particularly between 20 ppm and 100 ppm. This trend can be attributed to the increased driving force for mass transfer between the aqueous phase and the surface of the adsorbent, which facilitates more effective diffusion of Fe ions to the available active sites. The higher availability of Fe ions at elevated concentrations allows for more active sites to be occupied, resulting in a higher q_e [15]. However, at 120 ppm, a slight drop in q_e is observed, signifying the onset of adsorbent site saturation. This indicates that most of the active sites are already occupied and further increases in Fe concentration do not lead to higher adsorption. In fact, excessive concentrations might lead to pore blockage or competition among Fe ions for limited active sites, thus reducing adsorption efficiency. On the other hand, the percentage removal of Fe decreases as the initial concentration increases. This inverse relationship is likely due to the fixed 0.01g adsorbent dosage being inadequate to handle excess Fe ions at higher concentrations, resulting in a total Fe being adsorbed [16]. These findings show the importance of balancing initial metal concentration with appropriate adsorbent dosage to maximize both removal efficiency and adsorption capacity.

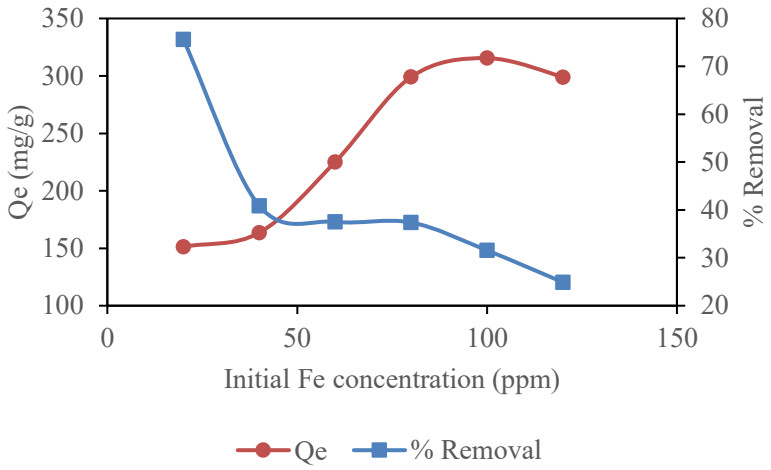


Figure 5 *Effect of initial Fe concentration on adsorption capacity and % removal of Fe.*

As shown in Fig. 6, the effect of contact time on Fe adsorption using activated carbon was evaluated. The results indicate that increasing contact time leads to a corresponding increase in both q_e and percentage removal. However, the rate of increase begins to taper after 120 min, suggesting that the adsorption process is nearing equilibrium. The minimal difference in Fe removal observed between 120 and 180 min further supports this, indicating that extending the contact time beyond 120 min provides only marginal improvement in adsorption performance [17]. Therefore, 120 min can be considered the optimal contact time for efficient Fe adsorption under the specified experimental conditions.

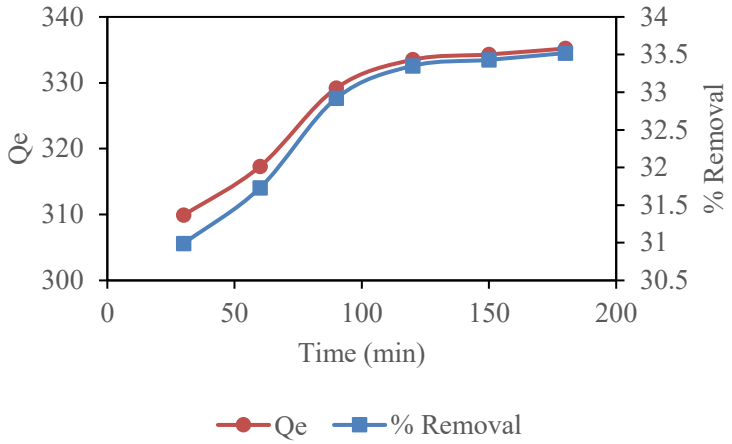


Figure 6 *Effect of contact time on adsorption capacity and % removal of Fe.*

Conclusion

Activated carbon was successfully synthesized from palm kernel shell using calcium chloride derived from cockle shell through an eco-friendly activation process. Optimization using the Taguchi L_9 orthogonal array identified the best synthesis conditions as 600°C, 60 min, and 0.25 M calcium chloride. The resulting activated carbon exhibited a high surface area of 435.64 m^2/g, good pore volume, and small pore size, with FESEM images revealing compact sub-spherical particles containing well-arranged circular pores. The Fe adsorption performance depended on adsorbent dosage, initial concentration, and contact time. Lower adsorbent dosage increased adsorption capacity (q_e), reaching 450.2 mg/g at 0.005 g, while higher dosages achieved greater overall removal efficiency (up to 43.91%). Lower initial Fe concentrations resulted in higher removal efficiency (75.65% at 20 ppm), whereas higher concentrations yielded greater q_e values. Longer contact times improved adsorption until equilibrium was reached between 120-180 min, with a maximum q_e of 335.2 mg/g. Overall, maximum Fe removal occurred at low initial concentrations and high adsorbent dosages, while maximum adsorption capacity was achieved at low adsorbent dosages and high Fe concentrations, with 120 min sufficient to reach near equilibrium.

Acknowledgement

This research was supported in full with Kurita Asia Research Grant (24Pmy227) provided by Kurita Water and Environment Foundation.

References

[1] A. Nayeem, F. Mizi, M.F. Ali, J.H. Shariffuddin, Utilization of cockle shell powder as an adsorbent to remove phosphorus-containing wastewater. Environ. Res. (2023). 216. 114514. https://doi.org/10.1016/j.envres.2022.114514

[2] N.S. Mohd Isha, F. Mohd Kusin, N.M. Ahmad Kamal, S.N.M. Syed Hasan, V.L.M. Molahid, Geochemical and mineralogical assessment of sedimentary limestone mine waste and potential for mineral carbonation. Environ. Geochem. Health (2021). 43.5. 2065-2080. https://doi.org/10.1007/s10653-020-00784-z

[3] Z. Heidarinejad, M.H. Dehghani, M. Heidari, G. Javedan, I. Ali, M. Sillanpää, Methods for preparation and activation of activated carbon: a review. Environ. Chem. Lett. (2020). 18.2. 393-415. https://doi.org/10.1007/s10311-019-00955-0

[4] M.A. Islam, M.V. Jacob, E. Antunes, A critical review on silver nanoparticles: From synthesis and applications to its mitigation through low-cost adsorption by biochar. J. Environ. Manag. (2021). 281. 111918. https://doi.org/10.1016/j.jenvman.2020.111918

[5] A. Bhatnagar, W. Hogland, M. Marques, M. Sillanpää, An overview of the modification methods of activated carbon for its water treatment applications. Chem. Eng. J. (2013). 219. 499-511. https://doi.org/10.1016/j.cej.2012.12.038

[6] K. Udyani, D.Y. Purwaningsih, Chemical and Physical Activation Using a Microwave to Increase the Ability of Activated Carbon to Adsorb Dye Waste. J. Phys. Conf. Ser. (2021). 2117.1. 012030. https://doi.org/10.1088/1742-6596/2117/1/012030

[7] X.l. Long, P.y. Chen, X.y. Jin, Effect of modification with hydrobromic acid on the performance of activated carbon in the removal of hexavalent chromium from aqueous solution. Environmental Progress & Sustainable Energy (2023). 43. https://doi.org/10.1002/ep.14245

[8] T.V. Nagalakshmi, K.A. Emmanuel, C. Babu, C. Challari, P. Divakar, Preparation of Mesoporous Activated Carbon from Jackfruit PPI-1 Waste and Development of Different Surface Functional Groups. ILCPA (2015). 54. 189-200. https://doi.org/10.18052/

[9] H. Kristianto, A.A. Arie, R.F. Susanti, M. Halim, J.K. Lee, The effect of activated carbon support surface modification on characteristics of carbon nanospheres prepared by deposition precipitation of Fe-catalyst. IOP Conf. Ser.: Mater. Sci. Eng. (2016). 162.1. 012034. https://doi.org/10.1088/1757-899X/162/1/012034

[10] M. Wei Tze, M. Aroua, M. Szlachta, Palm Shell-based Activated Carbon for Removing Reactive Black 5 Dye: Equilibrium and Kinetics Studies. Bioresour. (2016). 11. 1432-1447. https://doi.org/10.15376/biores.11.1.1432-1447

[11] M.P. Divya, S. Krishnamoorthi, R. Ravi, V.G. Jenner, K. Baranidharan, M. Raveendran, P. Hemalatha, Preparation and characterization of activated carbon from commercially important bamboo species in north eastern India. Adv. Bamboo Sci. (2025). 11. 100148. https://doi.org/10.1016/j.bamboo.2025.100148

[12] A.R. Hidayu, N. Muda, Preparation and Characterization of Impregnated Activated Carbon from Palm Kernel Shell and Coconut Shell for CO_2 Capture. Procedia Eng. (2016). 148. 106-113. https://doi.org/10.1016/j.proeng.2016.06.463

[13] U. Kouakou, A.S. Ello, J.A. Yapo, A. Trokourey, Adsorption of iron and zinc on commercial activated carbon. J. Environ. Chem. Ecotoxicol (2013). 5.6. 168-171

[14] T.M. Alslaibi, I. Abustan, M.A. Ahmad, A.A. Foul, Kinetics and equilibrium adsorption of iron (II), lead (II), and copper (II) onto activated carbon prepared from olive stone waste. Desalination Water Treat. (2014). 52.40-42. 7887-7897. https://doi.org/10.1080/19443994.2013.833875

[15] R.S. Brishti, R. Kundu, M.A. Habib, M.H. Ara, Adsorption of iron(III) from aqueous solution onto activated carbon of a natural source: Bombax ceiba fruit shell. Results Chem. (2023). 5. 100727. https://doi.org/10.1016/j.rechem.2022.100727

[16] S.O. Okonji, L. Yu, J.A. Dominic, D. Pernitsky, G. Achari, Adsorption by Granular Activated Carbon and Nano Zerovalent Iron from Wastewater: A Study on Removal of Selenomethionine and Selenocysteine. (2021). 13.1. 23

[17] M.E. Wahyuhadi, R.A. Kusumadewi, R. Hadisoebroto, Effect of Contact Time on The Adsorption Process of Activated Carbon from Banana Peel in Reducing Heavy Metal Cd and Dyes Using a Stirring Tub (Pilot Scale). IOP Conf. Ser.: Earth Environ. Sci. (2023). 1203.1. 012035. https://doi.org/10.1088/1755-1315/1203/1/012035